Reliability Engineering and System Safety 245 (2024) 110000

Contents lists available at ScienceDirect

Reliability Engineering and System Safety

journal homepage: www.elsevier.com/locate/ress

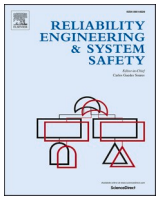

Virtual modelling based fragility assessment of structures under bushfire propagation

Zhiyi Shi [a], Yuan Feng [a,*], Mark G. Stewart [b], Wei Gao [a,*]

[a] Centre for Infrastructure Engineering and Safety (CIES), School of Civil and Environmental Engineering, The University of New South Wales, Sydney, NSW 2052, Australia
[b] School of Civil and Environmental Engineering, University of Technology Sydney, Ultimo, NSW 2007, Australia

ARTICLE INFO

Keywords:
Probability-based fragility assessment
Bushfire hazard
Virtual modelling
Uncertainty quantification
Extended-support vector regression
Climate change

ABSTRACT

Driven by increased human activities in rural-urban interfaces, the construction of residential or commercial buildings in these areas is experiencing a notable growing trend. In comparison to those built in urban regions, these structures, constructed in rural-urban interfaces, are in closer proximity to natural vegetation, therefore facing a heightened bushfire risk. The timely execution of Structural Protection Plans (SPP) is of utmost importance in the case of bushfire threats, where a swift response within a short timeframe is necessary, considering the diverse fragility characteristics of structural components. To address this, the present study introduces a novel framework for assessing the fragility of typical residential structures under both low and high wind speed conditions, specifically focusing on three key structural components: window frames, walls, and roofs. The assessment of structural probability-based fragility is performed using the newly developed limit state function and takes into account the influence of multiple non-deterministic factors, including vegetative conditions, wind speed, different temperature thresholds of structural components, and fire response time. Furthermore, to enable rapid prediction of structural probability-based fragility on the fireground, a virtual modelling (VM) technique, named extended support vector regression (X-SVR), is introduced and incorporated into the proposed fragility assessment framework. The efficiency and accuracy of this virtual modelling technique in assessing the bushfire fragility of structures under different wind speed intervals have been investigated and validated through a comprehensive case study of a real Australian house. The proposed framework is poised to provide valuable insights into optimizing SPP by swiftly identifying the most fragile structural components in practice.

1. Introduction

In recent decades, bushfires have resulted in significant human casualties and extensive property losses on a global scale. The 2020 Australian bushfire season led to the destruction of 3094 residential properties and the burning of over 17 million hectares of land [1], setting a new record for the extent of damage caused by bushfires. The majority of the reported damaged structures were located in areas close to dense natural vegetation [2]. Such an environment poses a significant bushfire risk to surrounding structures due to the flammable nature of vegetation [3], as illustrated in Fig. 1. In the face of bushfire threats, it becomes critically important for individuals to grasp the fragility of their structures to bushfires. It can assist individuals in knowing the arrival time of these fires and deciding when to implement a pre-prepared Structural Protection Plan (SPP), especially when firefighting resources are limited. The SPP, which is recommended by the NSW Rural Fire Service, includes measures such as closing doors and windows, lowering bushfire shutters, activating sprinklers to moisten the yard and roof, and disconnecting the gas and electricity supply, amongst other measures [4].

While the fragility of structures in the face of floods [7,8], earthquakes [9], and hurricanes [10,11] has been extensively studied, there has been limited investigation into the fragility assessment of building structures during bushfires. Most structures have a limited ability to withstand high-temperature environments. When exposed to direct flame contact or high heat radiation, they become highly fragile and may quickly lose their normal functionality. This state of compromised functionality is also commonly referred to as the exceeding of the limit

* Corresponding authors.
E-mail addresses: yuan.feng1@unsw.edu.au (Y. Feng), w.gao@unsw.edu.au (W. Gao).

https://doi.org/10.1016/j.ress.2024.110000
Received 30 October 2023; Received in revised form 8 January 2024; Accepted 5 February 2024
Available online 9 February 2024

state of serviceability. For instance, metal roofs and alloy window frames may quickly undergo large deformation, while timber walls may undergo charring.

In order to reduce the fragility of structures due to bushfire, it's imperative to promptly execute SPP before structural functionality is compromised. To this end, two key metrics, Structural Failure Time (SFT) and Fire Response Time (FRT), are employed to measure the fragility of structures during a bushfire. SFT is defined as the time span from the ignition of a bushfire until the structures start to sustain damage, whereas FRT represents the duration needed to carry out SPP. The fragility of structures can ultimately be evaluated by determining the probability that the FRT exceeds the SFT. Evaluating the fragility of structures, in the context of bushfire, is a complex task. It can be affected by a multitude of factors, such as:

- Temperature Thresholds of Structures [12]: This term denotes the highest temperature that structures can withstand. When these temperature thresholds are surpassed, structures are likely to be damaged and lose their normal functionality. Typically, structures built with fire-resistant materials or protected well by firefighting measures have a longer SFT, which consequently reduces structural fragility.
- Execution of SPP [13]: This term refers to the duration needed to carry out the SPP, otherwise known as the FRT. Multiple factors can impact the FRT, including the experienced level of the individuals involved and the preparation of SPP. A thoroughly prepared SPP can decrease the FRT, thereby reducing the fragility of structures. As demonstrated by Henok et al. [14], while 24 % of residents in Wildland-Urban Interface (WUI) communities choose to stay and protect their homes during bushfire incidents, the adequacy of their preparedness for SPPs raises concerns.
- Weather Conditions [15]: Weather conditions, particularly wind speed, significantly impact bushfire features such as the rate, intensity, and direction of bushfire spread. These factors, in turn, impact the fragility of structures. Typically, strong wind conditions tend to accelerate the spread rate, causing the firefront to reach structures more rapidly than under mild wind conditions. This results in a shorter SFT, necessitating a quicker execution of SPPs. To emphasize this point, the fragility of structures under both strong and mild wind scenarios is assessed concurrently in this study.
- Vegetation Conditions [15,16]: Factors such as moisture content, height, density, and type of vegetation significantly affect bushfire features and, subsequently, the fragility of structures. For instance, the intensity of a firefront burning in dry and dense vegetation tends to be much higher than that in wet and sparse vegetation, resulting in a stronger heat release rate and heat radiation. This can cause the firefront to damage structures from a greater distance, leading to a shorter SFT.

To simulate bushfire propagation while taking into account the aforementioned factors, it is first necessary to determine a suitable bushfire model. Generally, bushfire models can be classified into three categories: fully physical, semi-physical, and empirical models. Each category is distinguished by the mechanisms it uses to simulate bushfire propagation. Empirical models, such as the classical Rothermel fire spread model [17] and various fire spread equations tailored to different types of vegetation fuel reviewed in [18], are constructed based on historical bushfire datasets or experiments, without involving any physical mechanisms of bushfires. While empirical equations allow for computationally efficient simulation, the predicted bushfire features may lack reliability due to the approximate nature of the simulation process. To assess the impact of the wind field, arguably the most significant factor influencing bushfire features, a dynamic terrain-shaped wind field can be incorporated into the empirical model, resulting in a semi-physical model - the level set bushfire model in the Fire Dynamics Simulator (FDS) [19]. The advent of high-performance computing has facilitated the development of several computational fluid dynamics-based fully physical bushfire simulation models, including the Lagrangian particle model, boundary fuel model in FDS [19]. The full physical models provide a rigorous description of turbulent flows and combustion reaction kinetics, enabling the simulation of the intricate interaction between fire, fuel, weather, and topography with high spatiotemporal resolution. Based on these various models, numerous studies have been undertaken to examine the impact of various vegetation and environmental parameters, such as wind speed [20], the spatial distribution characteristics of vegetation [21,22], and the moisture content within the vegetation [23,24], on bushfire features. Beyond the scope of vegetation and environment, the impact of bushfire on the performance of residential buildings [25], and critical infrastructures [26] such as the traffic network [27] and the power grid [28] have been widely studied recently.

Previous studies have made significant contributions to our understanding of bushfire features and their impact on our society. However, there is still a lack of a unified framework for assessing the fragility of structures from the perspective of uncertain bushfire propagation, which is closer to real-world conditions. To address this, the current study proposes a novel Probability-based Fragility Assessment Framework (PFAF) for the structures in the context of bushfire, taking into account the non-deterministic nature of vegetation and environmental conditions. For obtaining a reliable outcome, the full physical bushfire model in FDS is utilized to simulate bushfire propagation. Additionally, a virtual modelling (VM) technique – the Extended Support Vector Regression (X-SVR) model – is introduced to mitigate the heavy computational burden caused by the full physical model. Essentially, the X-SVR is a type of supervised Machine Learning (ML) technique [29,30,31]. It stands out from other ML techniques in its ability to efficiently and accurately capture the nonlinear statistical correlation between bushfire features and concerned responses in an explicit manner, based on the dataset.

(a) (b)

Fig. 1. (a) House engulfed in flames [5]; (b) Proximity of bushfires to properties [6].

The robustness and capacity of the X-SVR have been proven in solving complex nonlinear engineering challenges, such as elastoplastic analysis [32], nonlinear geometric-material analysis [33,34], impact load analysis [35,36,37], structural dynamic fracture analysis [38], nonlocal damage for quasi-brittle materials [39,40]. Considering the highly nonlinear nature of bushfire propagation, the capacity of the X-SVR technique in solving the fragility of structures by analysing the relationship between vegetation and environmental factors and the concerned structural response "SFT" marks a novel attempt in the context of bushfire. Ultimately, the proposed Virtual Modelling aided Probability-based Fragility Assessment Framework (VM-PFAF) can utilize this statistical correlation to rapidly update the monitoring "SFT" responses by analysing ever-changing vegetation and environmental conditions in the fireground. This rapid prediction allows individuals involved to stay up-to-date with the latest bushfire developments, thereby enabling a more efficient decision-making process.

The structure of this study is as follows: Section 2 offers an in-depth overview of the research methodology employed. This section encompasses detailed descriptions of the process for evaluating the probability-based fragility of structures, the adopted probability theory, and an elucidation of the virtual modelling technique. Subsequently, Section 3 showcases the efficiency of the proposed framework in predicting the fragility of structures, illustrated through a real individual house in an Australian WUI community. Section 4 highlights the limitations and scope for the current study and finally, the main findings are concluded in Section 5.

2. Virtual modelling aided structural probability-based bushfire fragility assessment

In this study, FDS [19] is utilized as the numerical simulation tool to simulate bushfire propagation and capture the dynamic temperature response of structures. FDS is a computational fluid dynamics (CFD) simulation platform that employs the large eddy simulation (LES) approach to model fire-driven fluid flow, based on the Navier–Stokes equations.

The adiabatic surface temperature AST is adopted to represent the temperature response of structures. It is initially introduced by Ulf Wickström [41] and is a hypothetical temperature at which the net heat flux between the gas and solid structure is zero. At a given time t after a bushfire is ignited, AST can be calculated using the following equation:

$$\varepsilon_s\left[q_{\text{inc}}(t)-\sigma T_{AST}(t)^4\right]+h_c\left[T_g(t)-T_{AST}(t)\right]=0 \tag{1}$$

where $\varepsilon_s[q_{\text{inc}}(t)-\sigma T_{AST}(t)^4]$ denotes the net radiative heat flux of the surface of a solid structure at time t; $h_c[T_g(t)-T_{AST}(t)]$is the net convective heat flux at time t; ε_s represents the surface emissivity; $q_{\text{inc}}(t)$ denotes the incident radiative heat flux onto the surface; σ is the Stefan–Boltzmann constant; h_c represents the convective heat transfer coefficient; and $T_g(t)$ is the surrounding gas temperature at time t.

The non-deterministic vegetation conditions are characterized by four vegetation parameters, which are modelled as random variables. These four vegetation parameters include vegetation surface-to-volume ratio x_{SAV}, vegetation moisture content $x_{moi.}$, vegetation height $x_{thick.}$, and vegetation bulk density $x_{dens.}$. More details regarding these vegetation parameters can be found in [42]. Moreover, the non-deterministic environmental conditions are also represented by random wind speed x_{wind} and random ambient temperature $x_{temp.}$. Finally, a random vector $\mathbf{x}$, encapsulating these six random variables, can be formulated to represent a non-deterministic bushfire event.

$$\mathbf{x}=\left[x_{SAV},x_{moi.},x_{thick.},x_{dens.},x_{temp.},x_{wind}\right]\in\Re^6 \tag{2}$$

Ultimately, the AST on the structural surface in a non-deterministic bushfire event can be expressed as:

$$\varepsilon_s\left[q_{\text{inc}}(\mathbf{x},t)-\sigma T_{AST}(\mathbf{x},t)^4\right]+h_c\left[T_g(\mathbf{x},t)-T_{AST}(\mathbf{x},t)\right]=0 \tag{3}$$

It is evident that the T_{AST} is no longer solely dependant on time t but is also dependant on the random vector $\mathbf{x}$. Consequently, the T_{AST}, at time t, is no longer a deterministic value but rather a function of the random vector $\mathbf{x}$.

Utilizing the temperature response T_{AST}, the bushfire-adapted limit state function of structures for assessing the structural fragility was first proposed. Generally, a structure consists of various components with respective capacities to withstand high-temperature environments. When the temperature response T_{AST} first exceeds the temperature thresholds of the structures at time T_0, the structure loses its primary functionality and enters a state of failure, indicating the SFT. It is important to note that, although a structural component may serve multiple functions and have corresponding temperature thresholds for each function, this study considers only the primary function of each component. For example, the primary function of an alloy window frame is to secure the glass in place. If large deformation in the window frame occurs at T_0, leading to the inability to hold the glass securely, T_0 is then regarded as the temperature threshold for the window frame. Fig. 2 demonstrates the process of determining SFT according to the temperature threshold of structural primary function.

Ultimately, the SFT can be expressed as:

$$SFT(\mathbf{x})=\min(t|T_{\text{AST}}(\mathbf{x},t)\geq T_{\text{th}}) \tag{4}$$

where the T_{th} denotes the temperature threshold corresponding to the primary function of each structural component.

FRT is another important factor in the formulation of the limit state function for structures under bushfire. It represents the time required to execute SPPs and can be influenced by various factors, including the proficiency of operators and their preparedness. In this study, the FRT is also considered as a non-deterministic parameter that follows a specific probability distribution. However, there is a lack of studies investigating the appropriate probability representation for the FRT. Herein, considering the non-negative nature of the FRT and the successful application of the lognormal distribution in modelling probability distribution in relevant real-life scenarios [43,44], it is assumed that the FRT follows a lognormal distribution with a coefficient of variation of 0.05. This assumption is based on both the statistical properties of the lognormal distribution and its applicability to similar time-related variables in practical applications. Ultimately, the limit state function $g(\mathbf{x})$ of structures under bushfire propagation can be formulated as:

$$g(\mathbf{x})=SFT(\mathbf{x})-FRT \tag{5}$$

A value of $g(\mathbf{x})$ less than or equal to zero indicates that the SPP cannot be fully implemented before structural damage occurs, and thus to be deemed as fragile. Therefore, the fragility of structures (P_f) can be estimated by Eq. (6).

$$P_f=\Pr[g(\mathbf{x})\leq 0] \tag{6}$$

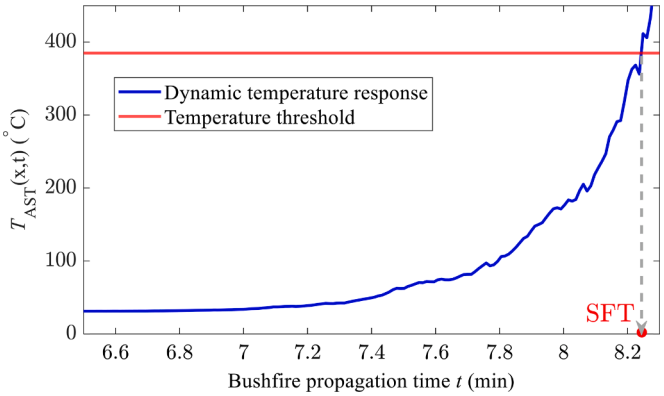

Fig. 2. Determination of SFT.

Monte Carlo Simulation (MCS) is a widely utilized and powerful tool to estimate the probability-based fragility of structures P_f in a non-deterministic bushfire event. By generating numerous bushfire samples randomly, MCS can provide a reliable probability density distribution of desired responses in an uncertain event, such as [45,46]. To approximate the fragility of structures P_f using MCS, numerous bushfire samples are initially generated randomly from the probability distribution across the domain of the random vector $\mathbf{x}$, and modelled using FDS. The numerical simulations aim to obtain the responses: SFTs of the individual components. By determining the value of the limit state function $g(\mathbf{x})$ for structural components, the fragility of each structural component P_f can be calculated using Eq. (6).

Despite its conceptual and algorithmic simplicity, the MCS entails a substantial computational cost. Typically, to achieve a reliable approximation, a large number of samples is required. This process can lead to extensive computational time, particularly in cases where the physics-based model is numerically demanding, such as bushfire simulation using FDS. Although the computational cost for running MCS can be reduced through parallel computing strategies on high-performance clusters, the limited accessibility to such clusters restricts its widespread availability. Furthermore, in the ever-changing fireground, some structural responses need to be assessed based on the latest bushfire information, such as SFT. These often exhibit a significant time sensitivity, preventing the time-consuming MCS from being utilized to estimate these time-sensitive structural responses.

To address the aforementioned gaps in MCS, surrogate models are being extensively studied to reduce the computational cost when analysing complex engineering structures. As a type of surrogate model, the X-SVR is adopted to substantially reduce the computational cost for rapid prediction of structural fragility with real-time data in the fireground. It enables the approximation of the inherent relationship between variable vegetation inputs and the SFT output, bypassing physics-based models and facilitating rapid predictions. The mathematical fundamentals of X-SVR method can be regarded as an extension of the kernelized Doubly Regularized Support Vector Machine (DrSVM) [47].

Given the training dataset with the training size n and input random variables m, the training dataset with input $\mathbf{x}_{train}$ and output $\mathbf{y}_{train}$ can be expressed as:

$$\mathbf{x}_{train} = \begin{bmatrix} \mathbf{x}^1_{trial-1} & \mathbf{x}^2_{trial-1} & \cdots & \mathbf{x}^m_{trial-1} \\ \mathbf{x}^1_{trial-2} & \mathbf{x}^2_{trial-2} & \cdots & \mathbf{x}^m_{trial-2} \\ \cdots & \cdots & \cdots & \cdots \\ \mathbf{x}^1_{trial-n} & \mathbf{x}^2_{trial-n} & \cdots & \mathbf{x}^m_{trial-n} \end{bmatrix}; \mathbf{y}_{train} = \begin{bmatrix} y_{trial-1} & y_{trial-2} & \cdots & y_{trial-n} \end{bmatrix}^T \tag{7}$$

Nonlinear support vector regression, also referred to as kernelized support vector regression, is based on the core concept of mapping original input data points $\mathbf{x}_{trial-i}$, often linearly inseparable in the original feature space $\Re^m$, to a higher-dimensional feature space through the application of a kernel function, as expressed in Eq.(A1). In this study, a new polynomial kernel function, combining the Padé expansion for diagonally approximating exponential function e^x and the Gaussian kernel function is introduced.

$$K(\mathbf{x}_i, \mathbf{x}_j) = \frac{\sum_{k=0}^{K} P_k(\mathbf{x}_i)^T P_k(\mathbf{x}_j)}{\exp\left(\sigma \| \mathbf{x}_i - \mathbf{x}_j \|_2^2\right)} \tag{8}$$

where $\mathbf{x}_i \in \Re^{m\times 1}$represents the i^{th} random vector and is defined in $[-1,1]$ after normalizing the original data, $\sigma$is the positive kernel scale parameter, K is the order of the polynomial, and$P_k(\mathbf{x}_i)$is the Padé expansions for e^x [48] and can be expressed as:

$$P_k(\mathbf{x}) = \frac{\frac{(2K-k)!}{k!(K-k)!}\mathbf{x}^k}{\frac{(2K-k)!}{k!(K-k)!}(-\mathbf{x})^k} \tag{9}$$

In the higher-dimensional feature space, there exist multiple hyperplanes that can effectively separate distinctive classes. The objective of X-SVR is to identify the optimal hyperplane that maximizes the distance to the nearest data points. To determine this optimal hyperplane, the following quadratic programming problem must be solved:

$$\min_{\mathbf{p}_k,\mathbf{q}_k,\gamma,\boldsymbol{\xi},\widehat{\xi}} : \frac{\lambda_1}{2}\left(\| \mathbf{p}_k \|_2^2 + \| \mathbf{q}_k \|_2^2\right) + \lambda_2 \mathbf{e}_n^T(\mathbf{p}_k + \mathbf{q}_k) + \frac{C}{2}\left(\boldsymbol{\xi}^T\boldsymbol{\xi} + \widehat{\xi}^T\widehat{\xi}\right)$$
$$s.t. \begin{cases} \left(\mathbf{K}(\mathbf{p}_k - \mathbf{q}_k) - \gamma\mathbf{e}_n^T\right) - \mathbf{y}_{train} \le \varepsilon\mathbf{e}_n^T + \boldsymbol{\xi} \\ \mathbf{y}_{train} - \left(\mathbf{K}(\mathbf{p}_k - \mathbf{q}_k) - \gamma\mathbf{e}_n^T\right) \le \varepsilon\mathbf{e}_n^T + \widehat{\xi} \\ \mathbf{p}_k, \mathbf{q}_k, \widehat{\xi}, \boldsymbol{\xi} \ge \mathbf{0}_n \end{cases} \tag{10}$$

where $\mathbf{p}_k, \mathbf{q}_k \in \Re^{n\times 1}$are the two non-negative variables of kernelized X-SVR model; $\lambda_1, \lambda_2 > 0$are tuning parameters that control the balance between the classification performance and feature selection; $\boldsymbol{\xi}$ and $\widehat{\xi}$ are the non-negative slack variables; $\mathbf{y}_{train}$ is the structural output; and $\gamma \in \Re$ is the bias.

For simplicity, the above quadratic programming problem can be reformulated to the following optimization problem [49]:

$$\min_{\mathbf{d}_k} : \frac{1}{2}\mathbf{d}_k{}^T\mathbf{E}_k\mathbf{d}_k - \mathbf{n}_k{}^T\mathbf{d}_k \; s.t. \; \mathbf{d}_k \ge \mathbf{0}_{4n} \tag{11}$$

where $\mathbf{E}_k \in \Re^{4n\times 4n}$and $\mathbf{n}_k \in \Re^{4n}$, whose details are represented in Appendix A:

Let $\mathbf{d}_k^* \in \Re^{4n}$ be the obtained solution for Eq.(11), the optimal hyperplane can be expressed as the following regression function:

$$\widehat{f}(\mathbf{x}) = (\mathbf{p}_k - \mathbf{q}_k)^T\widehat{\mathbf{k}}(\mathbf{x}) - \widehat{\mathbf{e}}_k{}^T\widehat{\mathbf{M}}_k\mathbf{d}_k^* \tag{12}$$

For any updated bushfire characteristics $\mathbf{x}_{upd.} = [\mathbf{x}^1_{upd.}, \mathbf{x}^2_{upd.}, \ldots, \mathbf{x}^m_{upd.}]^T$, the corresponding SFT $\widehat{f}(\mathbf{x}_{upd.})$ can be predicted by:

$$\widehat{f}(\mathbf{x}_{upd.}) = (\mathbf{p}_k - \mathbf{q}_k)^T\widehat{\mathbf{k}}(\mathbf{x}_{upd.}) - \widehat{\mathbf{e}}_k{}^T\widehat{\mathbf{M}}_k\mathbf{d}_k^* \tag{13}$$

To this end, the implementation of the proposed kernelized X-SVR model follows the key steps as described below:

1. Generate n bushfire samples $\mathbf{x}_{MCS} = \Re^{n\times 6}$ randomly from the predefined probability distribution across the domain of the random vector $\mathbf{x}$.
2. Select l bushfire samples $\mathbf{x}_{train}$ using Sobol's sequence from the whole bushfire samples $\mathbf{x}_{MCS}$.
3. Simulate l bushfire samples on the FDS platform and determining the SFT of the investigated structural components in each sample to form the initial training dataset ($\mathbf{x}_{train}$,$\mathbf{y}_{train}$).
4. Train the X-SVR model based on the initial training dataset ($\mathbf{x}_{train}$,$\mathbf{y}_{train}$) to obtain the relationship between random vector $\mathbf{x} = [x_{SAV}, x_{moi.}, x_{thick.}, x_{dens.}, x_{temp.}, x_{wind}]$ and SFT.
5. For validating the accuracy of the predicted result $\mathbf{y}_{pred.}$, the actual result $\mathbf{y}_{MCS}$ of the whole 1000 bushfire samples is obtained through the FDS. With $\mathbf{y}_{MCS}$ as benchmark, goodness of fit (R^2) and root mean square error (RMSE) of the $\mathbf{y}_{pred}$ is calculated to judge the convergence of the trained X-SVR model corresponding to the training size of l.
6. After obtaining the converged X-SVR model, the SFTs of any structural component can be estimated according to Eq. (13) under any newly generated bushfire samples.
7. Based on the newly estimated SFTs, the probability-based fire fragility of the corresponding structural component can be reassessed and updated finally.

To provide a visual representation of the aforementioned steps, a flowchart depicting the process is presented in Fig. 3.

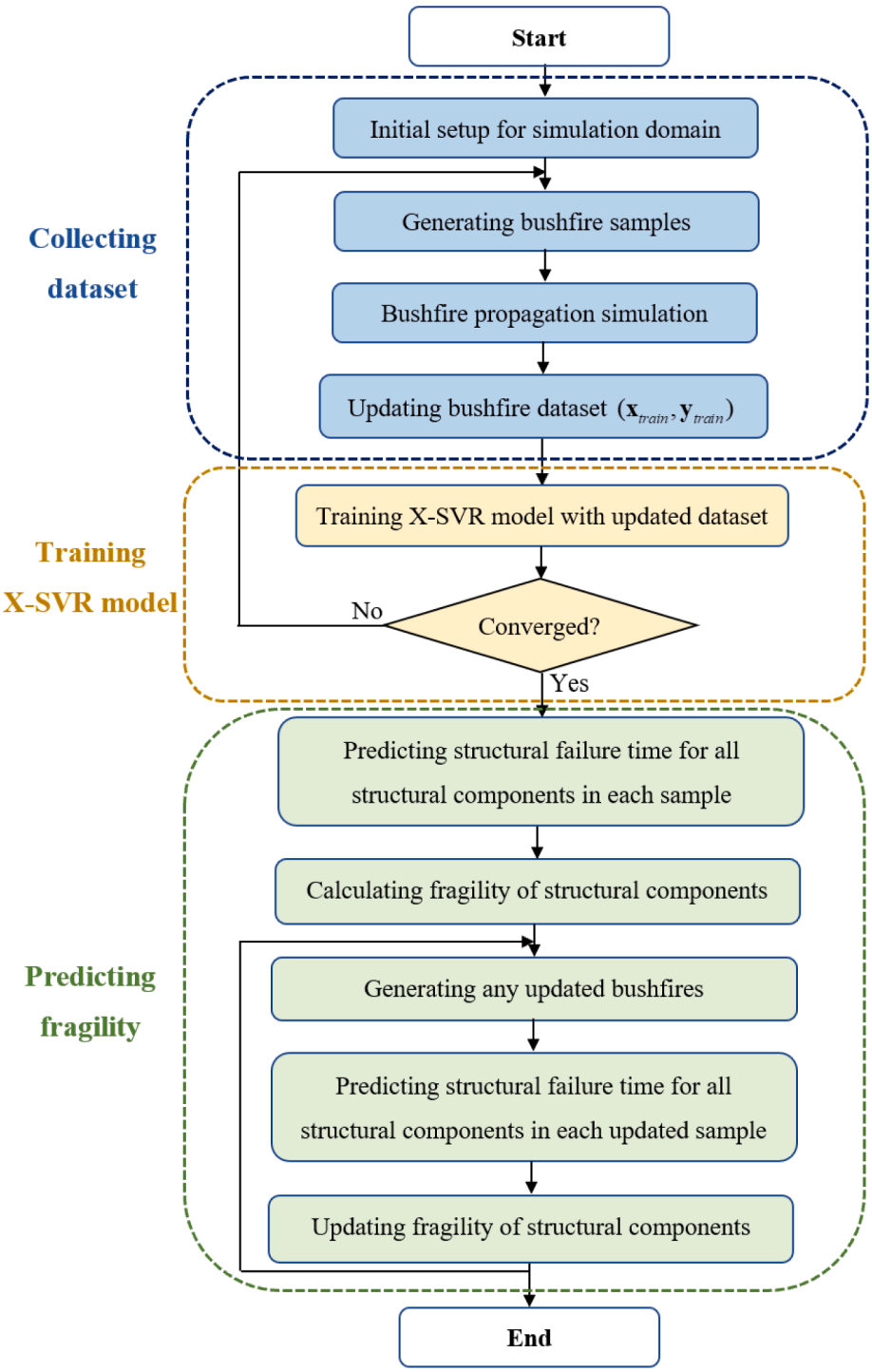

Fig. 3. The flowchart for assessing the fragility of structures.

3. Case study

In this study, the proposed framework is utilized to predict the fragility of three key structural components in a real residential house: the window frame, wall, and roof. This house was destroyed in the 2020 Perth bushfire [50], as shown in Fig. 4. Numerical simulations, including the training of surrogate model, were conducted on a single workstation. This workstation is equipped with an Intel(R) Xeon(R) Gold 5215 CPU @ 2.5 GHz, has 10 cores, and is supported by 192 GB of RAM.

To simulate the bushfire propagation, a simulation domain with dimensions of 200 m in length, 42 m in width, and 10 m in height is established, as illustrated in Fig. 5. To monitor the temperature response of the three structural components, three detectors are positioned on the surfaces of the analysed structural components, as shown in Fig. 5. Fig. 5 showcases the visual representation of the bushfire spread at four distinct time points following its ignition.

To evaluate the failure status of structural components, a deterministic criterion is required, which further aids in assessing the probability-based fragility of these structural components. For this purpose, the temperature threshold is treated as the deterministic boundary value to determine the Structural Failure Time (SFT). The three temperature thresholds for the three structural components are defined in Table 1.

(a) (b)

Fig. 4. (a) The house before the fire [51]; (b) in the fire [50].

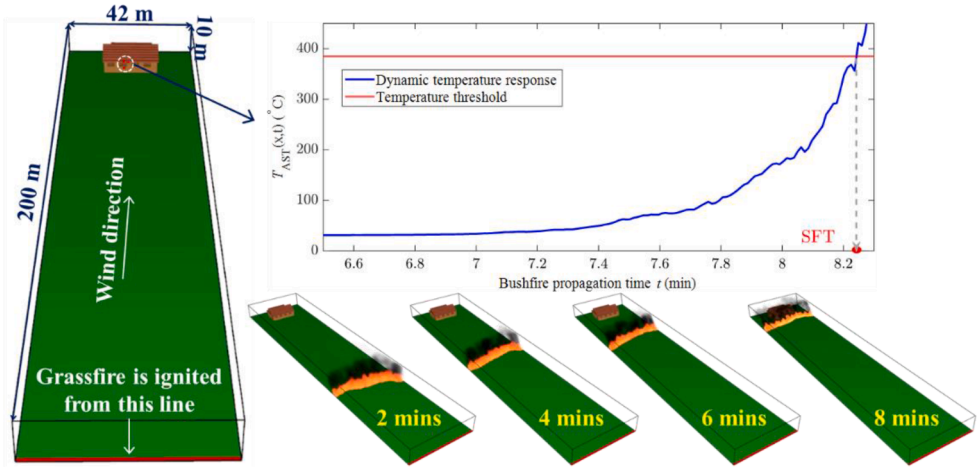

Fig. 5. The simulation domain of the residential house.

Table 1
The temperature thresholds for the three analysed structural components [52].

Component	Materials	Damage type	Temperature threshold
Window frame	Metal	Thermal softening	321°C
Wall	Timber	Ignited and burning	281°C
Roof	Metal	Thermal softening	385°C

Additionally, the statistics of the random vegetation and environmental variables, listed in the random vector **x**, have been summarized in Table 2.

Table 2
The statistical characteristics of the random variables in the random vector **x** [42].

	Random variables	Distribution	Mean	COV
Random environmental conditions	Wind speed (m/s)	Normal	13 (Strong wind scenario) 6 (Mild wind scenario)	0.04
	Ambient temperature (°C)		28	
	Surface-to-volume ratio (1/m)	Lognormal	4920	
Random vegetation conditions	Height (m)	Beta	0.6	
	Moisture content	Normal	0.08	
	Bulk density (kg/m^3)	Uniform	0.8	

To generate a dataset with input-output data pairs for training and verifying the surrogate model, numerous MCS bushfire samples are first randomly generated from the statistical distributions outlined in Table 2. The non-deterministic dynamic AST responses of the three structural components in the scenarios of both strong and mild winds are represented in Fig. 6. It can be observed that the consideration of uncertainty in the vegetation and environmental conditions significantly contributes to the non-deterministic SFTs.

To guarantee that the trained surrogate model can promptly regress a converged function to reliably express the impact of the random input vegetation and environmental data in the statistics of non-deterministic output SFT response, different training sample sizes are selected to observe the convergence trend. The statistics R^2 is used to quantify the performance of trained surrogate models under different training sizes. According to the results shown in Fig. 7, the size of the training samples is determined to be 40 % of the total sample size.

Based on the well-trained surrogate model, Fig. 8 demonstrates the comparison results of the graph of the probability density and the cumulative probability of the non-deterministic SFTs predicted by the surrogate model and simulated in FDS. Overall, the R^2 of the predicted results is well above 0.94 for all components in the scenarios of both strong and mild winds.

Additionally, Table 3 also lists the key statistical moments "mean" and "standard deviation" of the predicted random output SFTs. The maximum relative error (RE) of the predicted results is −3.25 % in the scenario of strong winds and −3.37 % in the scenario of mild winds.

Finally, the accuracy of the well-trained surrogate model is validated more thoroughly by predicting the SFTs of all bushfire samples. Fig. 9 demonstrates the predicted SFTs of components in all samples in the two

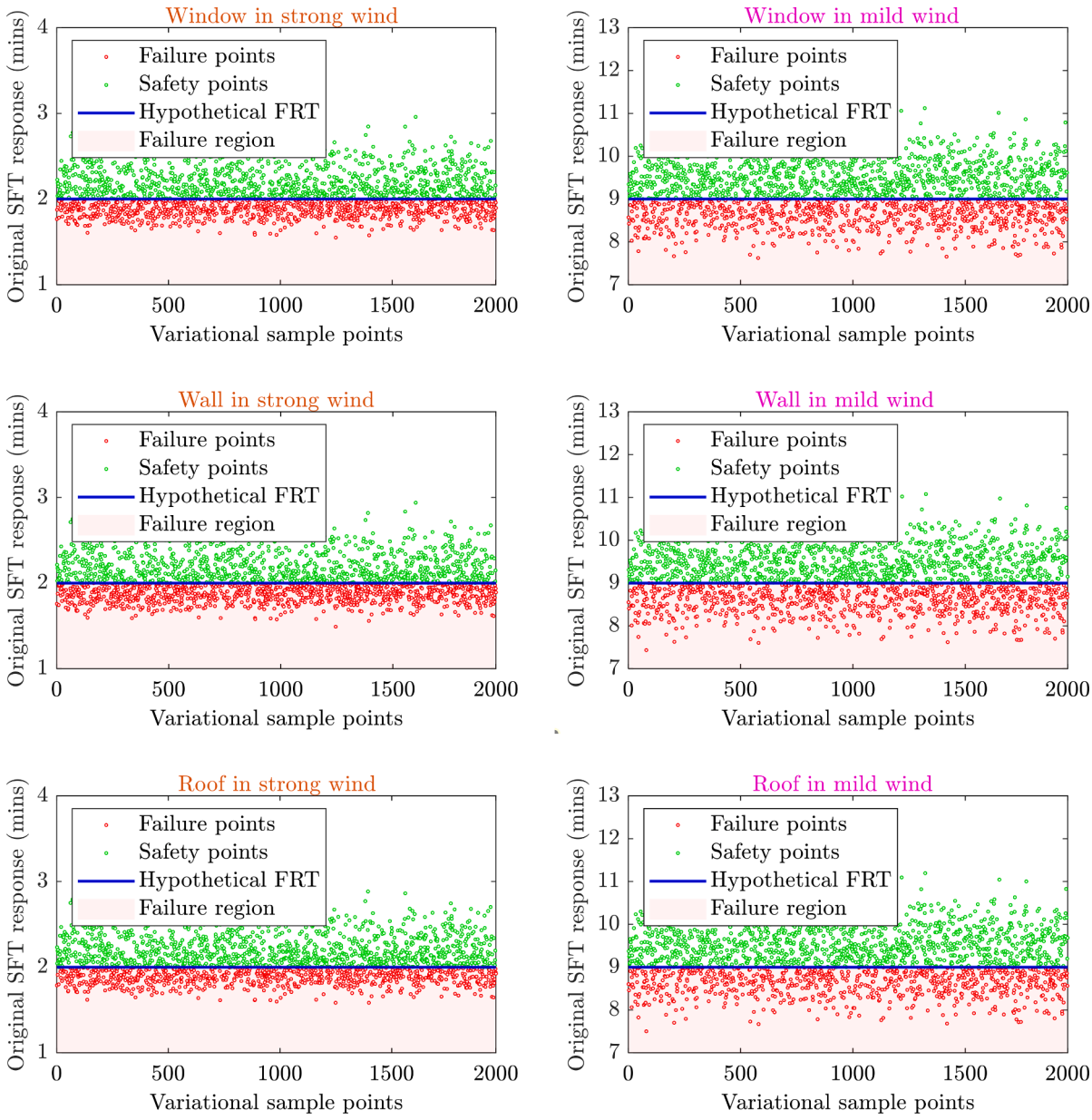

Fig. 6. The non-deterministic SFT responses in the scenarios of both strong and mild winds.

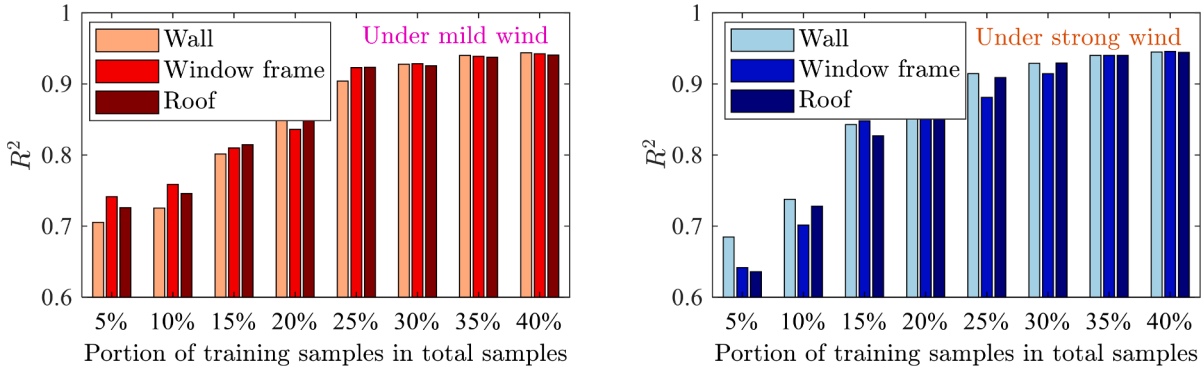

Fig. 7. The R^2 of the trained surrogate model under different training sample sizes.

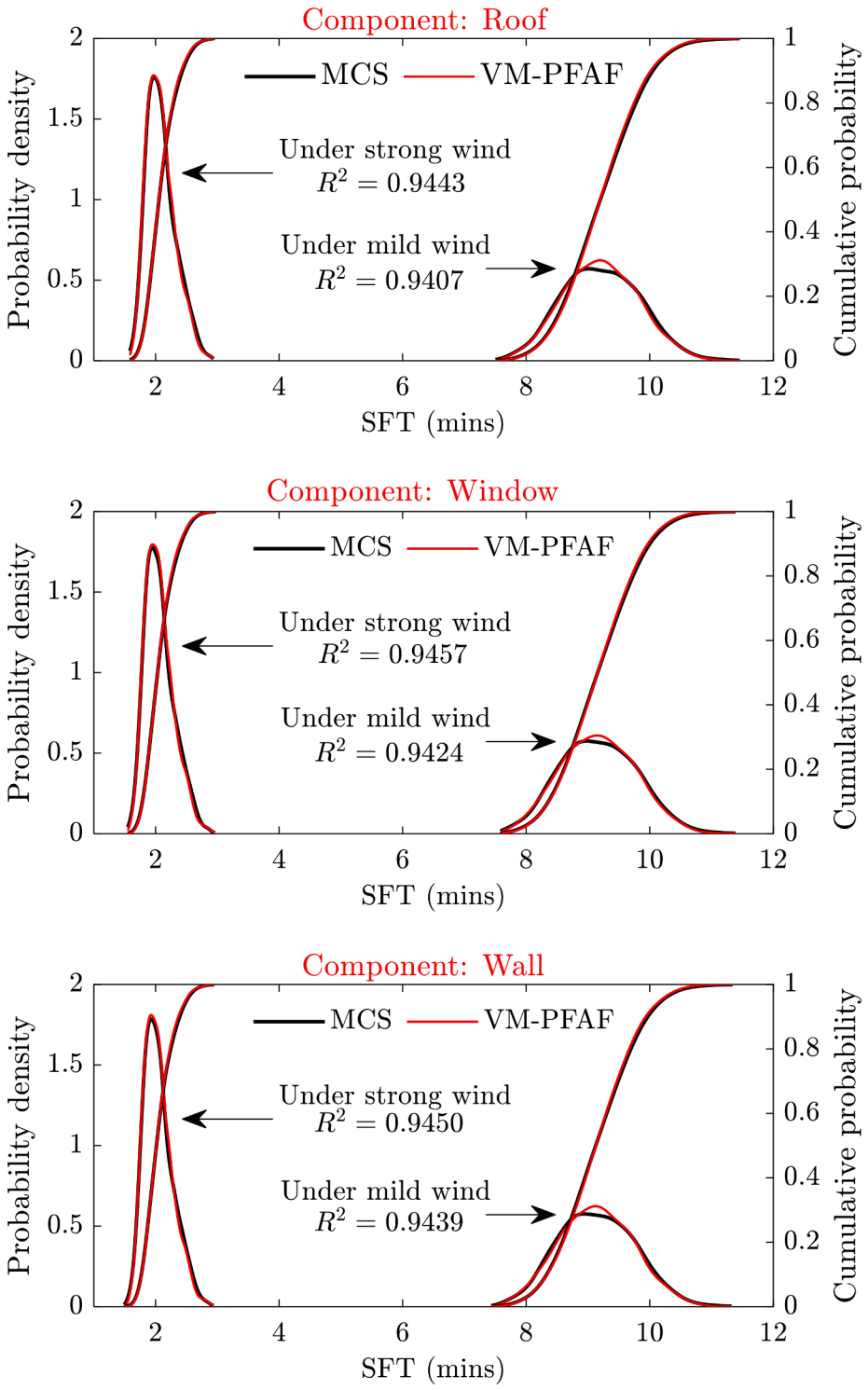

Fig. 8. The probability density and cumulative probability of the predicted SFTs.

Table 3
The statistical characteristics of the predicted SFTs.

Scenarios	Moments	Window		Wall		Roof	
		SFT (min)	RE (%)	SFT (min)	RE (%)	SFT (min)	RE (%)
Strong winds	Mean	2.06	−0.20	2.04	−0.20	2.09	−0.22
	Std.	0.23	−3.23	0.27	−3.25	0.23	−3.11
Mild winds	Mean	9.16	−0.09	9.13	−0.07	9.21	−0.06
	Std.	0.60	−2.96	0.60	−2.87	0.60	−3.37

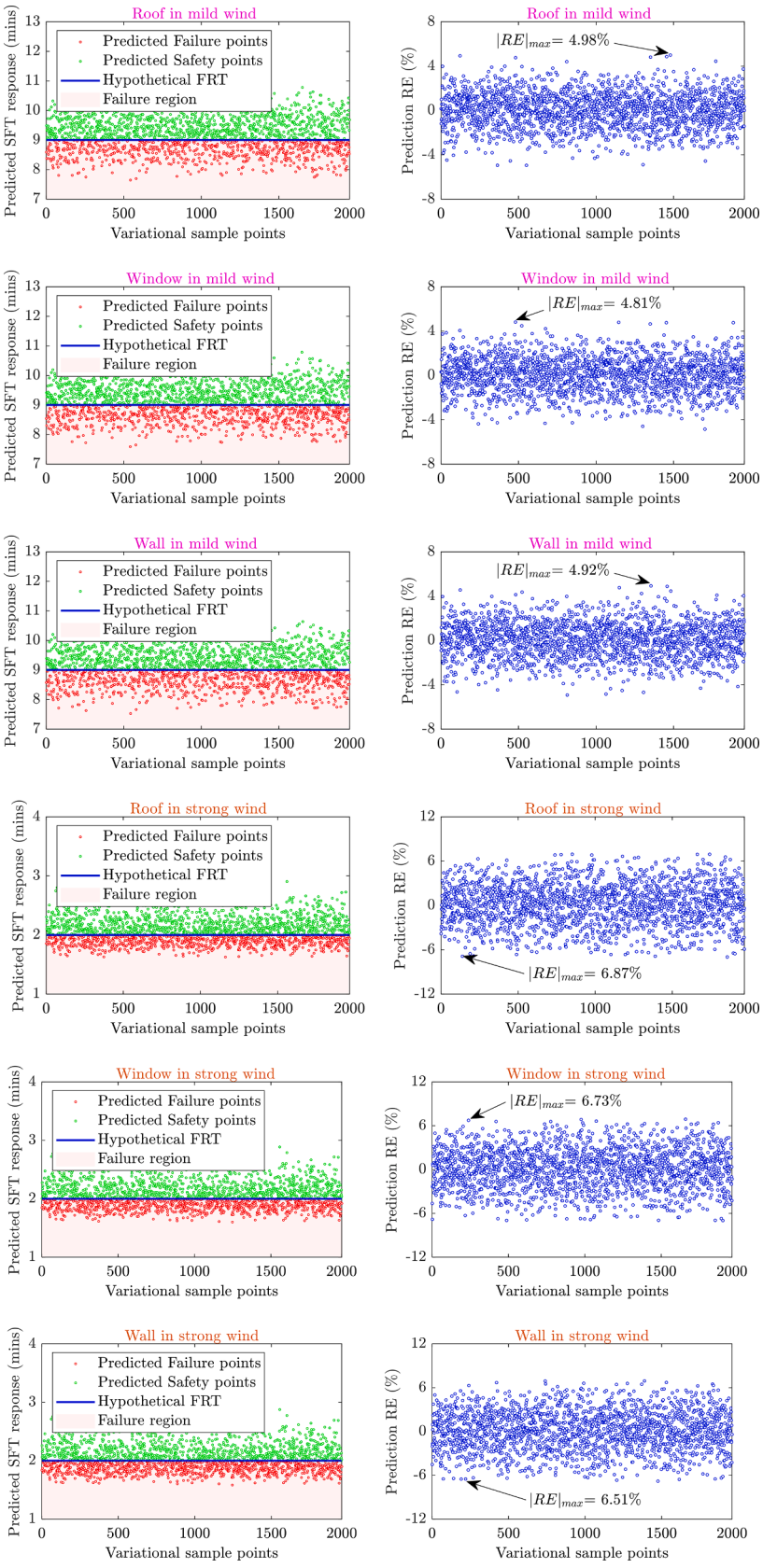

Fig. 9. The predicted SFTs and its RE in all samples under two wind scenarios.

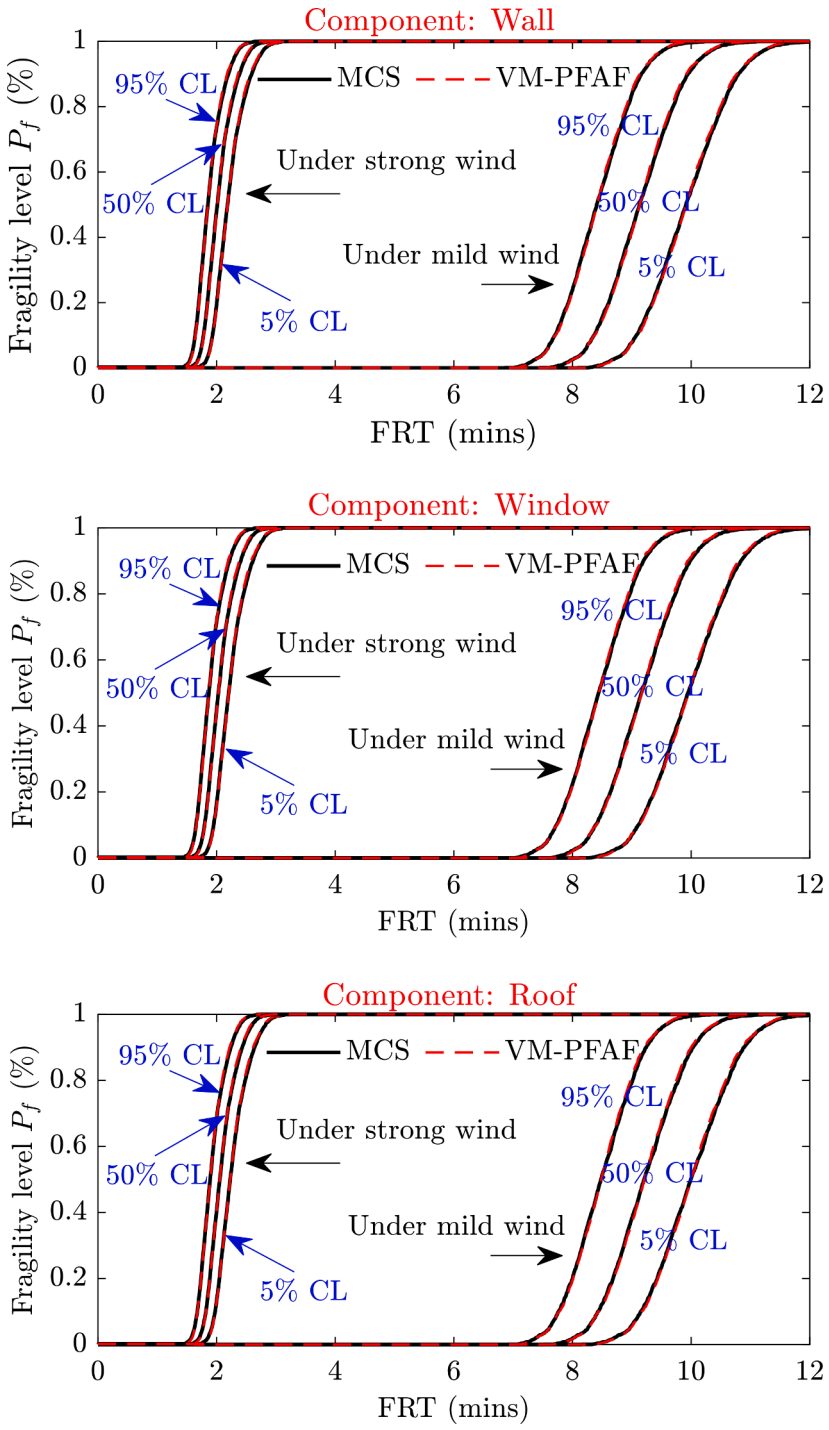

Fig. 10. The fragility curves of structural components at different confidence levels (CL) of FRT.

Table 4
The maximum allowable FRT required to ensure a 0 % fragility level.

Confidence level	Scenario	Window frame	Wall	Roof
5 % CL	Strong winds	1.7 min	1.6 min	1.7 min
	Mild winds	8.3 min	8.2 min	8.4 min
50 % CL	Strong winds	1.6 min	1.5 min	1.6 min
	Mild winds	7.6 min	7.5 min	7.7 min
95 % CL	Strong winds	1.5 min	1.4 min	1.5 min
	Mild winds	7.0 min	6.9 min	7.1 min

wind scenarios. The maximum RE is 6.87 % under strong winds and 4.98 % under mild winds. The RE of the predicted results is well restricted to within 5 % in most samples.

After verifying the accuracy and robustness of the well-trained surrogate model in predicting the output response SFT, the predicted SFTs can be considered reliable and utilized to further assess the fragility of structural components. Based on the definition of structural fragility in Eq. (6), the fragility curves of three structural components are plotted in Fig. 10. It is evident that wind conditions play a significant role in the fragility of structures. In the scenario of strong winds, to maintain a low fragility level of the structural components as in mild winds, the FRT need to be dramatically reduced from about 8 min to 2 min, which will

Table 5
The six newly generated bushfire samples.

Random variables	Mild wind scenario			Strong wind scenario		
	Sample 1	Sample 2	Sample 3	Sample 4	Sample 5	Sample 6
x_{wind} (m/s)	7	6	5	12	13	14
x_{temp}(°C)	29	28	29	28	30	31
x_{SAV} $(1/m)$	4700	4900	5700	4850	4900	5000
$x_{moi.}$	0.1	0.08	0.09	0.08	0.08	0.09
$x_{thick.}$ (m)	0.6	0.6	0.7	0.6	0.6	0.7
$x_{dens.}$ (kg/m^3)	0.8	0.8	0.9	0.8	0.8	0.9

undoubtedly put immense pressure on the operation of SPP.

To ensure all the structural protection measures are completed before the structures are damaged, Table 4 lists the maximum allowable FRTs under different CLs in both wind scenarios. It is observed that at the same CL, the maximum allowable FRTs under strong winds shrink from about 8 mins under mild winds to less than 2 mins. This implies that the SPP must operate much more efficiently and quickly on windy days to provide as much protection to the structure as possible.

It's worth noting that the proposed surrogate model can not only achieve accurate regression of the input-output relationship from the original sample dataset, but it can also predict the output response directly for newly generated bushfire samples outside of the original dataset by utilizing this relationship, without any additional time-consuming numerical simulation. To verify the accuracy and efficiency of the proposed surrogate model in predicting responses for new samples, Table 5 lists six newly generated bushfire samples: three in strong wind conditions and three in mild wind conditions.

The well-trained surrogate model is used to predict the SFTs of the three structural components under these 6 new bushfire samples. The predicted responses are listed in Table 6. In terms of computational efficiency, the computational time needed to numerically simulate a bushfire sample to obtain the SFT responses generally is about 1.5 h. However, this time can be shortened to several seconds when using the well-trained surrogate model to predict the same SFT responses. The efficiency of the proposed surrogate model in the non-deterministic output prediction is significant.

According to Table 6, the maximum allowable FRT in both strong and mild wind scenarios, which ensures a 0 % fragility level at 95 % CL, can also be re-assessed. In the scenario of strong winds, the maximum allowable FRT is 1.72 min. This number can be extended to 10.58 min in the scenario of mild winds.

To evaluate the relative influence of the six random variables on the SFT, a sensitivity analysis is performed. The standard deviations associated with these random variables, as shown in Table 2, are systematically adjusted to 0.8, 0.9, 1.1, and 1.2 times the original standard deviations σ_0, while maintaining the stable mean values. By utilizing the updated input information, the X-SVR model enables the rapid prediction of the updated SFT. The percentage variation in the standard deviation of the updated SFT is presented in Fig. 11, offering insights into the sensitivity of SFT to the different random variables.

Fig. 11 highlights the significant influence of the random wind speed x_{wind} on the SFT, not only under the strong wind conditions, but also under the mild wind conditions, surpassing the impact of other input variables. These findings are consistent with previous investigations conducted by Liu, Y. et al. [53], Anderson, K. et al. [54], and Clark, R.E. et al. [55], in which the considerable influence of wind on bushfire behaviours was also observed.

4. Scope and limitations

To quantify the probability-based fragility of generalized individual structures in WUI communities under the non-deterministic grassfire, this study introduces two time metrics - 'FRT' and 'SFT' - and proposes a grassfire-induced fragility assessment framework aided by an X-SVR machine learning technique. Within this framework, the fragility of structures is defined as the probability of non-deterministic FRT exceeding random SFT, without considering the impact of other factors, such as the detailed design of structures, the effectiveness of firefighting plans, and the feasibility of suppressing bushfires, on the fragility of structures. Therefore, this does not imply that a structure can be saved merely by completing the necessary defensive measures before the firefront damages the structures. In addition, the study also faces other limitations and scopes:

- For determining the failure status of structures by using the first-passage failure principle, a pre-set deterministic temperature threshold is required. If the structural temperature reaches or exceeds the pre-set temperature threshold for the first time, the structure can be defined as failed and the corresponding SFT can be determined. However, in practice, the derivation of temperature thresholds and its variability can be considerably more complex and highly non-deterministic, especially when considering the geometric-material uncertainty of the structural components and the height-dependant temperature distribution across all structural components.
- To simulate bushfire propagation, the full physical model in FDS is utilized. Due to numerical implementation challenges, this model does not consider the ember attack fire mechanism and includes only two fire attack mechanisms - direct flame contact and radiative heat.
- The spread of bushfire over grassland from one side to the structure was considered in the simulation. Situations in which bushfire approaches structures from multiple directions in the canopy are not considered in this study. However, the concept of time-based fragility assessment proposed in this study can still be extended to these scenarios in future research.

5. Conclusions

This paper presents a virtual modelling-aided framework for assessing the fragility of structures exposed to bushfires under both strong and mild wind conditions. The two key metrics "SFT" and "FRT" are introduced to define the fragility of structures, highlighting the

Table 6
The predicted SFT (min) in newly generated samples.

Components	Sample 1	Sample 2	Sample 3	Sample 4	Sample 5	Sample 6
Wall	8.27	8.73	10.20	2.60	1.96	1.72
Window frame	8.48	9.22	10.38	2.62	1.97	1.75
Roof	8.73	9.28	10.58	2.63	2.00	1.78

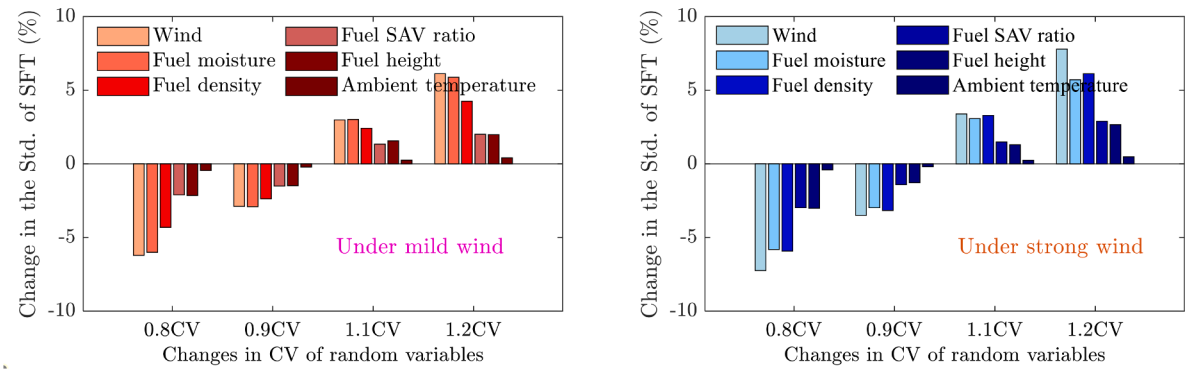

Fig. 11. Variation in the standard deviation of SFT corresponding to the change in CV of random variables.

important role of a well-prepared SPP in the mitigation of structural fragility. To mitigate the computational burden during the assessment of structural fragility, an advanced supervised machine learning technique-kernelized X-SVR model-is proposed to be a surrogate model. The X-SVR model can approximate the inherent relationship between SFT and random vegetation and environmental variables, achieving efficient prediction of structural response-SFT. The bushfire-adapted X-SVR model is also enhanced by introducing a novel kernel function which is derived through the Padé approximation of the exponential function. In practice, the proposed fragility assessment framework can efficiently and accurately predict the SFT of structures and evaluate the fragility of structures without any additional time-consuming numerical simulations. This can help to identify the most fragile structural components and optimize the operation of SPP in a time-sensitive fireground. Future studies will be focused on optimizing and refining the limit state function that governs the response of structures under bushfire propagation, to develop a more comprehensive assessment of structural fragility.

Data availability

No data was used for the research described in the article.

CRediT authorship contribution statement

Zhiyi Shi: Conceptualization, Software, Methodology, Validation, Formal analysis, Investigation, Writing – original draft, Visualization. **Yuan Feng:** Conceptualization, Software, Methodology, Writing – review & editing. **Mark G. Stewart:** Writing – review & editing, Supervision, Methodology. **Wei Gao:** Writing – review & editing, Supervision, Methodology, Resources.

Declaration of competing interest

The authors declare that they have no known competing financial interests or personal relationships that could have appeared to influence the work reported in this paper.

Acknowledgements

The work presented in this paper is supported by the Australian Research Council projects IH200100010, DP210101353, DP240102559, IH210100048 and the Australian Research Training Program Scholarship. The research work has been undertaken with the assistance of resources and services from the National Computational Infrastructure (NCI) Australia.

The authors would like to express our sincere thanks to the reviewers about their valuable comments and constructive suggestions.

Appendix A

A1. Mapping input data $\mathbf{x}_{trial-i}$ from a low-dimensional origin space $\Re^m$ to a higher-dimensional space through the application of a kernel function:

$$\mathbf{x}_{trial-i} = \left[\mathbf{x}^1_{trial-i}, \mathbf{x}^2_{trial-i}, \ldots, \mathbf{x}^m_{trial-i}\right]^T \mapsto \widehat{\mathbf{k}}(\mathbf{x}_{trial-i}) = \begin{bmatrix} \boldsymbol{\Phi}(\mathbf{x}_{trial-1})^T \boldsymbol{\Phi}(\mathbf{x}_{trial-i}) \\ \boldsymbol{\Phi}(\mathbf{x}_{trial-2})^T \boldsymbol{\Phi}(\mathbf{x}_{trial-i}) \\ \vdots \\ \boldsymbol{\Phi}(\mathbf{x}_{trial-n})^T \boldsymbol{\Phi}(\mathbf{x}_{trial-i}) \end{bmatrix} = \begin{bmatrix} K(\mathbf{x}_{trial-1}, \mathbf{x}_{trial-i}) \\ K(\mathbf{x}_{trial-2}, \mathbf{x}_{trial-i}) \\ \vdots \\ K(\mathbf{x}_{trial-n}, \mathbf{x}_{trial-i}) \end{bmatrix} \tag{A.1}$$

where $\widehat{\mathbf{k}}(\mathbf{x}_{trial-i})$is i^{th} the empirical feature vector; $\boldsymbol{\Phi}(\mathbf{x}_{trial-i})$is the implicit mapping function and $K(\mathbf{x}_{trial-i}, \mathbf{x}_{trial-j})$is the applied kernel function.

A2. In Eq. (10), $\mathbf{E}_k \in \Re^{4n\times 4n}$ and $\mathbf{n}_k \in \Re^{4n}$are represented as:

$$\begin{aligned} \mathbf{E}_k &= (\widehat{\mathbf{L}}_k + \mathbf{I}_{4n\times 4n})\widehat{\mathbf{U}}_k^{-1}(\widehat{\mathbf{L}}_k + \mathbf{I}_{4n\times 4n})^T + \widehat{\mathbf{M}}_k \widehat{\mathbf{e}}_k \widehat{\mathbf{e}}_k^T \widehat{\mathbf{M}}_k \\ \mathbf{n}_k^T &= \lambda_2 \mathbf{t}_k^T \widehat{\mathbf{U}}_k^{-1}(\widehat{\mathbf{L}}_k + \mathbf{I}_{4n\times 4n})^T - \varepsilon \widehat{\mathbf{e}}_k^T - \widehat{\mathbf{h}}_k^T \end{aligned} \tag{A.2}$$

where $\mathbf{I}_{4n\times 4n} \in \Re^{4n\times 4n}$ represents the identity matrix. $\widehat{\mathbf{U}}_k$,$\widehat{\mathbf{L}}_k$and$\widehat{\mathbf{M}}_k$are written as:

$$\widehat{\mathbf{U}}_k = \begin{bmatrix} \lambda_1 \mathbf{I}_{n\times n} & & & \\ & \lambda_1 \mathbf{I}_{n\times n} & & \\ & & C\mathbf{I}_{n\times n} & \\ & & & C\mathbf{I}_{n\times n} \end{bmatrix} \widehat{\mathbf{L}}_k = \begin{bmatrix} \mathbf{0}_{2n\times n} & \mathbf{0}_{2n\times n} & \mathbf{0}_{2n\times 2n} \\ -\mathbf{K} & \mathbf{K} & \mathbf{0}_{n\times 2n} \\ \mathbf{K} & -\mathbf{K} & \mathbf{0}_{n\times 2n} \end{bmatrix} \widehat{\mathbf{M}}_k = \begin{bmatrix} \mathbf{0}_{2n\times 2n} & \mathbf{0}_{2n\times n} & \mathbf{0}_{2n\times n} \\ \mathbf{0}_{n\times 2n} & \mathbf{I}_{n\times n} & \mathbf{0}_{n\times n} \\ \mathbf{0}_{n\times 2n} & \mathbf{0}_{n\times n} & -\mathbf{I}_{n\times n} \end{bmatrix} \tag{A.3}$$

The vectors, $\mathbf{t}_k$, $\widehat{\mathbf{e}}_k$and $\widehat{\mathbf{h}}_k$ are written as:

$$\mathbf{t}_k = \begin{bmatrix} \mathbf{e}_n \\ \mathbf{e}_n \\ \mathbf{0}_{2n} \end{bmatrix}, \widehat{\mathbf{e}}_k = \begin{bmatrix} \mathbf{0}_{2n} \\ \mathbf{e}_n \\ \mathbf{e}_n \end{bmatrix}, \widehat{\mathbf{h}}_k = \begin{bmatrix} \mathbf{0}_{2n} \\ \mathbf{y}_{train} \\ -\mathbf{y}_{train} \end{bmatrix} \tag{A.4}$$

where $\mathbf{0}_{n\times n} \in \Re^{n\times n}$ is the zero vector, $\mathbf{e}_n = [1, 1, ..., 1]^T \in \Re^{n\times 1}$, $\lambda_1, \lambda_2 > 0$ are tuning parameters that control the balance between the classification performance and feature selection, $C > 0$ represents the penalty constant, ε is the tolerable deviation between y_i and $\widehat{f}(\mathbf{x}_i)$. $\mathbf{K} \in \Re^{n\times n}$ is the kernel matrix containing the original training samples can be expressed as:

$$\mathbf{K} = \begin{bmatrix} K(\mathbf{x}_{trial-1}, \mathbf{x}_{trial-1}) & K(\mathbf{x}_{trial-1}, \mathbf{x}_{trial-2}) & \cdots & K(\mathbf{x}_{trial-1}, \mathbf{x}_{trial-n}) \\ K(\mathbf{x}_{trial-2}, \mathbf{x}_{trial-1}) & K(\mathbf{x}_{trial-2}, \mathbf{x}_{trial-2}) & \cdots & K(\mathbf{x}_{trial-2}, \mathbf{x}_{trial-n}) \\ \vdots & \vdots & \cdots & \vdots \\ K(\mathbf{x}_{trial-n}, \mathbf{x}_{trial-1}) & K(\mathbf{x}_{trial-n}, \mathbf{x}_{trial-2}) & \cdots & K(\mathbf{x}_{trial-n}, \mathbf{x}_{trial-n}) \end{bmatrix} \tag{A.5}$$

References

[1] Richards L, Brew N, Smith L. 2019-20 Australian bushfires—frequently asked questions: a quick guide. Canberra: ACT: Department of Parliamentary Services, Parliament of Australia; 2020. In: Library P, editorAvailable online at, https://www.aph.gov.au/About_Parliament/Parliamentary_departments/Parliamentary_Library/pubs/rp/rp1920/Quick_Guides/AustralianBushfires#:~:text=How%20many%20houses%20were%20destroyed,had%20been%20destroyed%20in%20NSW.

[2] Thomas DS, Butry DT. Areas of the U.S. wildland–urban interface threatened by wildfire during the 2001–2010 Decade. Nat Hazards 2013;71(3):1561–85. https://doi.org/10.1007/s11069-013-0965-7. Available at:.

[3] Price OF, Bradstock RA. The spatial domain of wildfire risk and response in the wildland urban interface in Sydney, Australia. Nat Hazards Earth Sys Sci 2013;13(12):3385–93. https://doi.org/10.5194/nhess-13-3385-2013. Available at:.

[4] *Prepare your home NSW rural fire service*. Available at: https://www.rfs.nsw.gov.au/plan-and-prepare/prepare-your-property (Accessed: 19 December 2023).

[5] Bragg, M.& (2016) *The Taylor bridge fire – what's next?, Millard and bragg - business and construction law - Oregon & Washington*. Available at: https://millardlaw.com/the-taylor-bridge-fire-whats-next/(Accessed: 30 October 2023).

[6] Di Giacomo Auriemma, Di and Auriemma, G. (2020) *Maxi Incendio in Sardegna: evacuate 250 case di due resort, Inews24.it*. Available at: https://www.inews24.it/2020/08/25/incendio-sardegna-evacuate-case/(Accessed: 30 October 2023).

[7] Caratozzolo V, Misuri A, Cozzani V. A generalized equipment vulnerability model for the quantitative risk assessment of horizontal vessels involved in Natech scenarios triggered by floods. Reliab Eng Syst Saf 2022;223:108504. https://doi.org/10.1016/j.ress.2022.108504.

[8] Rossi L, Casson Moreno V, Landucci G. Vulnerability assessment of process pipelines affected by flood events. Reliab Eng Syst Saf 2022;219:108261. https://doi.org/10.1016/j.ress.2021.108261.

[9] Argyroudis SA, Mitoulis SA. Vulnerability of bridges to individual and multiple hazards- floods and earthquakes. Reliab Eng Syst Saf 2021;210:107564. https://doi.org/10.1016/j.ress.2021.107564.

[10] Ma L, Christou V, Bocchini P. Framework for probabilistic simulation of power transmission network performance under hurricanes. Reliab Eng Syst Saf 2022;217:108072. https://doi.org/10.1016/j.ress.2021.108072.

[11] Amini K, Padgett JE. Probabilistic risk assessment of hurricane-induced debris impacts on coastal transportation infrastructure. Reliab Eng Syst Saf 2023;240:109579. https://doi.org/10.1016/j.ress.2023.109579.

[12] Syphard AD, Brennan TJ, Keeley JE. The importance of building construction materials relative to other factors affecting structure survival during wildfire. Internatl J Disaster Risk Red 2017;21:140–7. https://doi.org/10.1016/j.ijdrr.2016.11.011. Available at:.

[13] McLennan J, et al. Householders' safety-related decisions, plans, actions and outcomes during the 7 february 2009 victorian (Australia) wildfires. Fire Saf J 2013;61:175–84. https://doi.org/10.1016/j.firesaf.2013.09.003. Available at:.

[14] Asfaw HW, McGee TK, Correia FJ. Wildfire preparedness and response during the 2016 Arouca wildfires in rural Portugal. Internat J Disaster Risk Red 2022;73:102895. https://doi.org/10.1016/j.ijdrr.2022.102895. Available at:.

[15] Cheney P, Sullivan A. Grassfires: fuel, weather and fire behaviour. Collingwood, Vic: CSIRO Pub; 2008.

[16] Penman SH, et al. The role of defensible space on the likelihood of house impact from wildfires in forested landscapes of South Eastern Australia. Int J Wildland Fire 2019;28(1):4. https://doi.org/10.1071/wf18046. Available at.

[17] Rothermel RC. A mathematical model for predicting fire spread in wildland fuels. Ogden, UT: Intermountain Forest and Range Experiment Station; 1972.

[18] Or D, et al. Review of wildfire modeling considering effects on land surfaces. Earth Sci Rev 2023;245:104569. https://doi.org/10.1016/j.earscirev.2023.104569.

[19] McGrattan KB, Forney GP. Fire dynamics simulator: user's manual. Gaithersburg, MD: U.S. Dept. of Commerce, Technology Administration, National Institute of Standards and Technology; 2000.

[20] Cruz MG, et al. Evaluating the 10% wind speed rule of thumb for estimating a wildfire's forward rate of spread against an extensive independent set of observations. Environm Modell Software 2020;133:104818. https://doi.org/10.1016/j.envsoft.2020.104818. Available at:.

[21] Massetti A, et al. The vegetation structure Perpendicular Index (VSPI): a forest condition index for wildfire predictions. Remote Sens Environ 2019;224:167–81. https://doi.org/10.1016/j.rse.2019.02.004. Available at.

[22] Cruz MG, Sullivan AL, Gould JS. The effect of fuel bed height in grass fire spread: addressing the findings and recommendations of Moinuddin et al. (2018). Int J Wildland Fire 2021;30(3):215. https://doi.org/10.1071/wf19186. Available at:.

[23] Marino E, et al. Fuel bulk density and fuel moisture content effects on fire rate of spread: a comparison between FIRETEC model predictions and experimental results in shrub fuels. J Fire Sci 2012;30(4):277–99. https://doi.org/10.1177/0734904111434286. Available at.

[24] Cruz MG, Alexander ME, Kilinc M. Wildfire rates of spread in grasslands under critical burning conditions. Fire 2022;5(2):55. https://doi.org/10.3390/fire5020055. Available at:.

[25] Chulahwat A. Capturing building vulnerability to wildfires with graph theory. Nat Rev Earth Environ 2023;4(9):600. https://doi.org/10.1038/s43017-023-00426-9. –600.

[26] Modaresi Rad A, et al. Human and infrastructure exposure to large wildfires in the United States. Nat Sustain 2023;6(11):1343–51. https://doi.org/10.1038/s41893-023-01163-z.

[27] Arango E, et al. Dynamic thresholds for the Resilience assessment of road traffic networks to wildfires. Reliab Eng Syst Saf 2023;238:109407. https://doi.org/10.1016/j.ress.2023.109407.

[28] Perera ATD, Hong T. Vulnerability and resilience of urban energy ecosystems to extreme climate events: a systematic review and Perspectives. Renew Sustain Energy Rev 2023;173:113038. https://doi.org/10.1016/j.rser.2022.113038.

[29] Wang Q, et al. Polymorphic uncertainty quantification for engineering structures via a hyperplane modelling technique. Comput Methods Appl Mech Eng 2022;398:115250. https://doi.org/10.1016/j.cma.2022.115250.

[30] Wang Q, Feng Y, Wu D, Yang C, et al. Polyphase uncertainty analysis through virtual modelling technique. Mech Syst Signal Process 2022;162:108013. https://doi.org/10.1016/j.ymssp.2021.108013.

[31] Zhao E, et al. Advanced virtual model assisted most probable point capturing method for engineering structures. Reliab Eng Syst Saf 2023;239:109527. https://doi.org/10.1016/j.ress.2023.109527.

[32] Feng Y, et al. Machine learning aided stochastic elastoplastic analysis. Comput Methods Appl Mech Eng 2019;357:112576. https://doi.org/10.1016/j.cma.2019.112576.

[33] Feng Y, et al. Virtual modelling technique for geometric-material nonlinear dynamics of structures. Struct Safe 2023;100:102284. https://doi.org/10.1016/j.strusafe.2022.102284.

[34] Feng Y, Wu D, et al. Safety assessment for functionally graded structures with material nonlinearity. Struct Safe 2020;86:101974. https://doi.org/10.1016/j.strusafe.2020.101974.

[35] Feng Y, Wang Q, Yu Y, et al. Experimental-numerical-virtual (ENV) modelling technique for composite structure against low velocity impacts. Eng Struct 2023;278:115488. https://doi.org/10.1016/j.engstruct.2022.115488.

[36] Tian Y, et al. Nonlinear dynamic analysis of the graphene platelets reinforced porous plate with magneto-electro-elastic sheets subjected to impact load. Nonlinear Dyn 2023. https://doi.org/10.1007/s11071-023-09093-3 [Preprint].

[37] Feng Y, et al. Virtual modelling aided safety assessment for ductile structures against high-velocity impact. Eng Struct 2024;301:117373. https://doi.org/10.1016/j.engstruct.2023.117373.

[38] Liu Y, et al. Virtual modelling integrated phase field method for dynamic fracture analysis. Int J Mech Sci 2023;252:108372. https://doi.org/10.1016/j.ijmecsci.2023.108372.

[39] Feng Y, et al. Stochastic nonlocal damage analysis by a machine learning approach. Comput Meth Appl Mech Eng 2020;372:113371. https://doi.org/10.1016/j.cma.2020.113371.

[40] Feng Y, et al. Machine learning aided phase field method for fracture mechanics. Int J Eng Sci 2021;169:103587. https://doi.org/10.1016/j.ijengsci.2021.103587.

[41] WickstrÃm U. Adiabatic surface temperature and the plate thermometer for calculating heat transfer and controlling fire resistance furnaces. Fire Safe Sci 2008;9:1227–38. https://doi.org/10.3801/iafss.fss.9-1227. Available at:.
[42] Scott JH, Burgan RE. Standard fire behavior fuel models: a comprehensive set for use with rothermel's surface fire spread model. United States: CreateSpace Independent Publishing Platform; 2015.
[43] Sutton IS. Chapter 16 - reliability, availability, and maintainability. in Process risk and reliability management: operational intergity management. Oxford: Elsevier (Amsterdam); 2015.
[44] Westgate BS, et al. Large-network travel time distribution estimation for ambulances. Eur J Oper Res 2016;252(1):322–33. https://doi.org/10.1016/j.ejor.2016.01.004.
[45] Qin H, Mason M, Stewart MG. Fragility assessment for new and deteriorated portal framed industrial buildings subjected to tropical cyclone winds. Struct Safe 2023;100:102287. https://doi.org/10.1016/j.strusafe.2022.102287.
[46] Stewart MG, Li J. Risk-based assessment of BLAST-resistant design of ultra-high performance concrete columns. Struct Safe 2021;88:102030. https://doi.org/10.1016/j.strusafe.2020.102030.
[47] Wang Li, et al. THE DOUBLY REGULARIZED SUPPORT VECTOR MACHINE. Stat Sin 2006;16(2):589–615. JSTOR, http://www.jstor.org/stable/24307560. Accessed 14 Mar. 2023.
[48] Song C, Eisenträger S, Zhang X. High-order implicit time integration scheme based on Padé expansions. Comput Met Appl Mech Eng 2022;390:114436. https://doi.org/10.1016/j.cma.2021.114436. Available at:.
[49] Feng J, et al. Dynamic reliability analysis using the extended support vector regression (X-SVR). Mech Syst Signal Process 2019;126:368–91. https://doi.org/10.1016/j.ymssp.2019.02.027.
[50] Jrood TA. *Perth family only realised their home had burned down while watching the news, ABC News*. ABC News 2021. Available at: https://www.abc.net.au/news/2021-02-02/wooroloo-bushfire-emergency-in-perth-hills-enters-second-day/13111784 (Accessed: January 26, 2023).
[51] Mayes A. *Three houses burned down as out-of-control Perth Hills bushfire threatens more homes, ABC News*. ABC News 2021. Available at: https://www.abc.net.au/news/2021-02-01/bushfire-in-perth-hills-wooroloo-at-emergency-level/13109956 (Accessed: January 26, 2023).
[52] *Online materials information resource MatWeb*. Available at: https://matweb.com/(Accessed: 13 October 2023).
[53] Liu Y, et al. Parametric uncertainty quantification in the Rothermel model with randomised quasi-monte carlo methods. Int J Wildland Fire 2015;24(3):307. https://doi.org/10.1071/wf13097.
[54] Anderson K, Reuter G, Flannigan MD. Fire-growth modelling using meteorological data with random and systematic perturbations. Int J Wildland Fire 2007;16(2):174. https://doi.org/10.1071/wf06069.
[55] Clark RE, et al. Sensitivity analysis of a fire spread model in a chaparral landscape. Fire Ecol 2008;4(1):1–13. https://doi.org/10.4996/fireecology.0401001.